

# MATERIALE COMPOZITE PE BAZĂ DE MgO ȘI NANOPARTICULE METALICE PENTRU APLICAȚII CATALITICE

## COMPOSITE MATERIALS BASED ON MgO AND METALLIC NANOPARTICLES FOR CATALYTIC APPLICATIONS

I.V. MATSUKEVICH<sup>1</sup>, I. ATKINSON<sup>2</sup>, S.V. BASARAB<sup>1</sup>, G. PETCU<sup>2</sup>, S. PETRESCU<sup>2</sup>, V. PÂRVULESCU<sup>2</sup>  
V. FRUTH<sup>2\*</sup>,

<sup>1</sup>Institute of General and Inorganic Chemistry of the National Academy of Sciences of Belarus

<sup>2</sup>„Ilie Murgulescu” Institute of Physical Chemistry of the Romanian Academy

*The aim of the paper is to obtain nanocomposites based on magnesium oxide and metal nanoparticles, as well as to establish the influence of the preparation methods on the properties and photocatalytic activity of these materials. Magnesium oxide was obtained by two preparation methods namely precipitation and combustion synthesis. The obtained samples were characterized from the structural, morphologically and compositionally point of view. Further, nanocomposites based on obtained MgO, were prepared by reducing metal ions to zero-valent metal nanoparticles immobilized on the surface of the MgO carrier (Cu and Ni). The photocatalytic activity of the synthesized nanocomposites was evaluated by monitoring the degradation of amoxicillin (AMX) aqueous solution under irradiation (365 nm).*

*Scopul lucrării este obținerea nanocompozitelor pe bază de oxid de magneziu și nanoparticule metalice, precum și stabilirea influenței metodelor de preparare asupra proprietăților și activității fotocatalitice a acestor materiale. Oxidul de magneziu a fost obținut prin două metode de preparare și anume precipitare și combustie. Probele obținute au fost caracterizate din punct de vedere structural, morfologic și compozițional. În plus, s-au obținut nanocompozite pe bază de MgO prin reducerea ionilor metalici la nanoparticule metalice cu valență zero (Cu și Ni) immobilizate pe suprafața MgO. Activitatea fotocatalitică a nanocompozitelor sintetizate a fost evaluată prin monitorizarea degradării soluției apoase de amoxicilină (AMX) sub iradiere (365 nm).*

**Keywords:** MgO, metal nanoparticles, nanocomposite, photocatalytic activity

### 1. Introduction

Dyes and antibiotics are among of the main contaminants released to the environment through the wastewater and the pharmaceutical manufacturing plants. Due to their low biodegradability and high chemical stability in the water system their accumulation in the environment is of increasing concern [1]. Adsorption and photocatalysis are potential technologies for wastewaters treatment before discharging them into the environment.

MgO has received a lot of attention due to its outstanding properties at nanoscale as well as its applications in various fields such as eradicating harmful metallic ions from wastewater, catalyst support, antimicrobial material, refractory material and adsorbents etc [1-3]. Basic oxides play a major role in catalytic chemistry and MgO is one of the most privileged oxides in the field of catalysis. Its catalytic interest is based on its essentially basic surface character, which makes it an effective catalyst and catalyst support [4].

In order to obtain MgO nanostructures, several physico-chemical methods such as

ultrasonic [5], microwave [4], sol-gel technique [6-8], hydrothermal technique [9], chemical precipitation [3], and combustion method [10] are used.

Due to its outstanding properties MgO has been selected as one of the promising support metal catalyst [11]. The design of MgO support metal catalysts has attracted intensive interest as an alternative to improve the stability and surface chemistry of the MgO support and hence, to obtain distinctive structures, properties, and applications. Catalyst supports can stabilize active metals which results in synergistic properties because of the interfacial interaction between MgO support and nanometals. Moreover the leaching phenomenon or metal agglomeration can be avoided. The selectivity and activity of the catalyst especially at higher temperature can be influenced by the dispersion and physico-chemical properties of active metals on the support catalyst.

Photocatalytic process using magnesium oxide is considered to be an effective method for amoxicillin removal from aqueous solution [12]. It were reported a higher performances for MgO as photocatalyst in comparison with other oxide

\* Autor corespondent/Corresponding author,  
E-mail: [vfruth@gmail.com](mailto:vfruth@gmail.com)

materials as N-doped TiO<sub>2</sub>, Degussa P25, TiO<sub>2</sub>, ZnO, WO<sub>3</sub>, Fe<sub>2</sub>O<sub>3</sub>, BiVO<sub>4</sub> and graphitic carbon nitride (g-C<sub>3</sub>N<sub>4</sub>) used in degradation of different pollutants from water [13].

The present study aims to investigate the influence of synthesis procedure on the MgO properties as well as the influence of the metal nanoparticles type Me-MgO (Me=Ni, Cu) on the degradation of amoxicillin.

## 2. Experimental

### 2.1 Materials preparation

**MgO** The magnesium oxide powder was prepared by precipitation method using 0.5 M aqueous solution of magnesium nitrate, prepared from Mg(NO<sub>3</sub>)<sub>2</sub>·6H<sub>2</sub>O, and 0.5 M aqueous solution of NaOH as precipitating agent. Aqueous solution of NaOH as precipitation agent added to aqueous solution of magnesium nitrate in equimolecular ratio at a constant rate (about 1 ml/s) with constant stirring. After precipitation, the obtained gel-like precipitate was repeatedly washed with distilled water, filtered off and dried to constant weight at a temperature of 105° C. Magnesium oxide was obtained by calcining the dried gel at 550°C for 2 h. Then, the obtained sample was thoroughly milled.

**MgO\*** The magnesium oxide powder was prepared by a typical glycine-citrate-nitrate method (combustion synthesis) using 2 M aqueous solution of magnesium nitrate, prepared from Mg(NO<sub>3</sub>)<sub>2</sub>·6H<sub>2</sub>O, and the certain amount of glycine and citric acid at the molar ratio of carbon/nitrogen (C/N) of 0.25. The components were mixed together and then the solution was evaporated under constant stirring on a magnetic stirrer at the temperature of 200°C. During evaporation, the solution thickened and turned into a gel. The gel turned into caramel, which frothed and finally ignited in a single point. Front burning spread over almost the entire mass of the foamed intermediate in a few seconds. As a result of the combustion of the gel, a light brown powder was formed, which turned into a white powder after heat treatment in air at 550°C for 2 hours.

**MgO<sup>o</sup>-Me, MgO<sup>\*</sup>-Me (Me = Ni, Cu)** For the synthesis of porous materials based on MgO and metal nanoparticles, samples of magnesium oxide prepared by the precipitation method and glycine-citrate-nitrate method were used

First of all, the synthesis of zero-valent metal nanoparticles was carried out by chemical reduction. For this purpose 0.02 M aqueous solutions of metallic nitrates were prepared using Ni(NO<sub>3</sub>)<sub>2</sub>·6H<sub>2</sub>O and Cu(NO<sub>3</sub>)<sub>2</sub>·6H<sub>2</sub>O. The metallic nitrate solution was placed in a three-necked flask; into which nitrogen gas from a cylinder with high-purity nitrogen was fed through an underwater capillary with polished surface (O<sub>2</sub> content was no more than 0.001% by volume). After passing nitrogen for 30 minutes, a solution of NaBH<sub>4</sub> was added into

the flask from a dropping funnel at a rate of 2-3 mL / min with constant stirring on an IKA C-MAG HS-7 magnetic stirrer, where sodium borohydride was taken with a 50 % mole excess (with a volume ratio of 1:1). After the total volume of sodium borohydride solution was supplied to the reactor, an alcoholic suspension of magnesium oxide, which was prepared using 96% ethanol, previously purged with nitrogen and followed by processing this alcoholic suspension in an ultrasonic bath with an operating frequency of 17 ± 1.7 kHz for 20 min, was added to the formed mixture. The resulting mixture was also ultrasonic treated for 30 minutes, then filtered off and dried in air at 200°C for 3 hours. Then the obtained samples were carefully grinded.

### 2.2 Materials characterization

The XRD patterns were collected by means of a Rigaku Ultima IV diffractometer in parallel beam geometry. The source of the X-rays was a Cu tube ( $\lambda = 1.54056 \text{ \AA}$ ) operating at 40 kV and 30 mA. XRD data were recorded with a step size of 0.02 and a speed of 2° (2 $\theta$ )/min over a range of 10-80°. Rigaku's PDXL software package connected to the ICDD database was used for the phase identification and unit cell parameters calculation. The unit cell parameters were refined by whole-powder - pattern fitting method (WPPF) using PDXL software. Crystallite size has been calculated using Scherrer's formula along (200) direction.

$$D = k \cdot \lambda / (\text{FWHM}) \cdot \cos(\theta) \quad (1)$$

where:  $\lambda$  is wave length of the Cu K $\alpha$  radiation (1.54056 Å), FWHM is full width at half maximum of the intensity vs. 2 $\theta$  profile,  $\theta$  is Bragg's diffraction angle and k is the shape factor taken as 0.9.

Fourier transform infrared (FTIR) spectroscopy was carried out with a Nicolet Spectrometer 6700 FTIR, within 400–4000 cm<sup>-1</sup> range (the FTIR spectrum is provided in absorbance mode). The spectra were recorded from thin transparent (~20 mg/cm<sup>2</sup>) KBr pellets containing approximately 0.5 wt% samples. Pellets were prepared by compacting and vacuum-pressing an intimate mixture obtained by grinding 1 mg of substance with 200 mg KBr.

Elemental analysis of the prepared nanocomposites was carried out using a wavelength dispersive X-ray fluorescence (WDXRF) spectroscopy method using Rigaku ZSX Primus II spectrometer equipped with an X-ray tube with Rh anode, 4.0 kW power, with front Be window, thickness of 30  $\mu\text{m}$ . The XRF measurements were performed on the pressed pellets of 1 mm diameter under vacuum atmosphere. The sample carriers were analysed under vacuum atmosphere. The XRF data were analyzed using EZ-scan combined with Rigaku's SQX fundamental parameters software (standard

less) which is capable of automatically correcting all matrix effects, including line overlaps.

The morphology of the samples was observed by scanning electron microscopy (SEM) using a high-resolution microscope, FEI Quanta3 DFEG model, at an accelerating voltage of 20 kV, in high vacuum mode with Everhart–Thornley secondary electron (SE) detector coupled with energy dispersive X-ray (EDX) analysis. Samples preparation was minimal and consisted in immobilizing the material on a double-sided carbon tape, without coating.

The adsorption and texture properties of the samples were assessed by the volume method on a Micromeritics ASAP 2020 MP surface area and porosity analyzer (United States) from isotherms of low-temperature (–196°C) static physical adsorption–desorption of nitrogen. The specific surface area was determined by the single- and multiple-point Brunauer–Emmett–Teller method ( $A_{BET}$ ,  $m^2 g^{-1}$ ). The specific pore volume  $V_{sp,des}$  ( $cm^3 g^{-1}$ ), average pore diameter  $D_{sp,des}$  (nm), and the pore size distribution in the linear form were determined by the Barrett–Joyner–Halenda method from the desorption branch of the isotherm in terms of the model of cylindrical pores. Prior to being analyzed, the samples were vacuum-treated for 1 h at a temperature of 200°C and residual pressure of  $133.3 \times 10^{-3}$  Pa.

The UV-vis diffuse reflectance spectra were recorded on a JASCO V570 spectrophotometer. As reference, a certified reflectance standard, Spectralon, has been used and the measurements were carried out in the range 900–200 nm.

Photocatalytic properties of the samples were investigated by monitoring the degradation efficiency of amoxicillin (AMX) aqueous solution under irradiation (365 nm). The photocatalytic reaction was used as a model test to evidence the photocatalytic properties of samples. In a typical experiment with AMX, 20 mg of the catalyst

was dispersed in 10 mL AMX aqueous solution (30 mg/L). Prior to irradiation, the suspensions were kept in dark for 30 min under stirring to ensure the achievement of the adsorption–desorption equilibrium under ambient conditions. During irradiation, at increasing time intervals, aliquots of the suspension were withdrawn and filtered through a 0.45  $\mu m$  Millipore filter to remove the catalyst. The residual AMX concentrations in the filtrates were analysed by UV–visible spectrophotometer at specific absorption wavelength of AMX ( $\lambda=230$  nm). The degradation efficiency (DE) was calculated from the following equation  $DE (\%) = (A_0 - A_t)/A_0 \times 100$ , where  $A_t$  is absorption value obtained after a specific time ( $t=1, 3, 5$  h) and  $A_0$  was the absorbance recorded after dark experiment.

### 3. Results and discussion

#### 3.1. XRD

The XRD results of MgO samples obtained by both methods and MgO<sup>''</sup>-Me, MgO<sup>\*</sup>-Me (Me = Ni, Cu) nanocomposites are shown in Table 1 and Figure 1. According to Fig. 1 the diffraction lines at 36.93°, 42.88°, 62.30°, 74.50° and 78.43° were indexed as (111), (200), (220), (311), and (222) crystal planes of cubic MgO (JCPDS, 01-071-1176). In the case of MgO sample obtained by precipitation method (Fig.2a), besides diffraction lines assigned to MgO, the diffraction lines corresponding to Mg(OH)<sub>2</sub> (JCPDS, 00-900-3875) and NaCl (JCPDS, 00-005-0628) were also identified. The lattice parameters and the average crystallite size of the samples (MgO<sup>''</sup> and MgO<sup>\*</sup>-Me (Me = Ni, Cu) together with the estimated standard deviation (in the brackets) are listed in Table 1.

The lattice parameters of MgO oxide were compared with the reported values of MgO phase ( $a = b = c = 4.217$ , JCPDS, 01-071-1176). The increase of lattice parameters as well as the

Table 1

Lattice parameters and crystallite size of MgO obtained by both methods and nanocomposites based on MgO  
 Parametrii de rețea și dimensiunea de cristalit ale MgO, obținut prin ambele metode și nanocompozitelor pe bază de MgO

| Sample                | Lattice parameters (Å) MgO<br>a=b=c | Crystallite size (200)<br>(Å) | Unit cell<br>volume-V<br>(Å <sup>3</sup> ) |
|-----------------------|-------------------------------------|-------------------------------|--|
| MgO <sup>''</sup>     | 4.2134(5)                           | 190(3)                        | 74.79                                      |
| MgO <sup>*</sup>      | 4.2171(3)                           | 135(3)                        | 74.99                                      |
| MgO <sup>''</sup> -Cu | 4.2145(3)                           | 178(2)                        | 74.85                                      |
| MgO <sup>*</sup> -Cu  | 4.230(5)                            | 78(8)                         | 75.68                                      |
| MgO <sup>''</sup> -Ni | 4.2148(2)                           | 186(3)                        | 74.87                                      |
| MgO <sup>*</sup> -Ni  | 4.2165(3)                           | 123(6)                        | 74.96                                      |
| MgO JCPDS-01-071-1176 | 4.217                               | -                             | 74.99                                      |

volume of unit cell in the MgO\*-Cu sample obtained by combustion method, can be attributed to the substitution of Cu<sup>2+</sup> (ionic radius 0.73 Å) for Mg<sup>2+</sup> (ionic radius 0.72 Å) that requires a local expansion of the lattice to accommodate the Cu<sup>2+</sup> ion in the MgO structure [14]. The average crystallite size of MgO calculated from the broadening of (200) diffraction line was between 130-190 Å. The crystallite size was influenced by the synthesis conditions, a decrease of crystallite in the case of samples obtained by combustion method was observed.

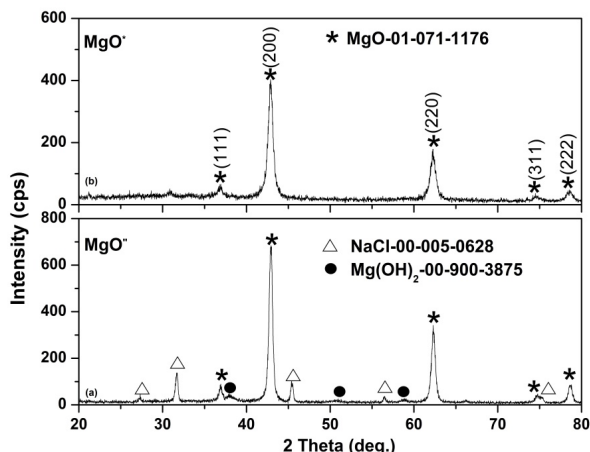


Fig. 1 - XRD patterns of MgO obtained by precipitation (a) and combustion (b) methods / Difractogramele de raze X ale MgO obținut prin metodele: (a) precipitare și (b) combustie.

### 3.2. FTIR Spectroscopy

In Figure 2 FT-IR spectra of MgO obtained by both methods are presented. It is well known that H<sub>2</sub>O and CO<sub>2</sub> molecules are easily chemisorbed onto MgO surface when exposed to the atmosphere thus the bands in the range of 1350–1640 cm<sup>-1</sup> were attributed to the deformation mode of physisorbed water molecules and the broad band at 3400 cm<sup>-1</sup> was attributed to stretching vibrations –OH groups. In addition, very weak band corresponding to the adsorption of gas phase CO<sub>2</sub> is visible around 2425 cm<sup>-1</sup>. The major vibrations at 467, 521 and 625 cm<sup>-1</sup> confirm the presence of Mg-O stretching vibrations of Mg-O-Mg bonding. Bands at 3440, 1637, 1400 and 521 cm<sup>-1</sup> were assigned to Mg(OH)<sub>2</sub> and 3629, 1119, 842 and 793 cm<sup>-1</sup> confirm the presence of MgCO<sub>3</sub> in the samples [17]

### 3.3 X-ray fluorescence (XRF) measurements

X-ray fluorescence analysis was used to determine the concentration of nanoparticles in the synthesized nanocomposites. The results are presented in Table 2.

### 3.4. Textural properties

The nitrogen adsorption/desorption isotherms curves are shown in Fig. 3 and estimated corresponding textural parameter values are listed

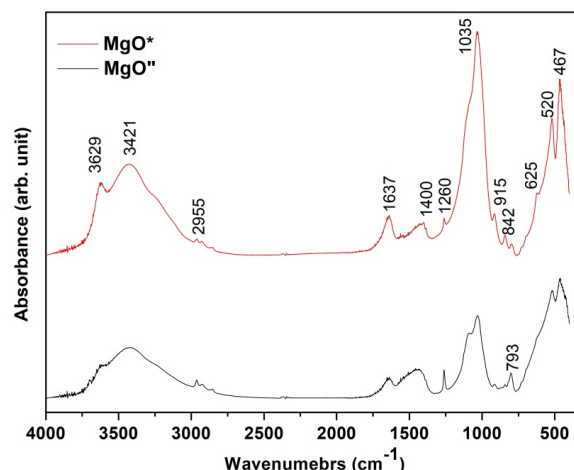


Fig. 2 - FTIR spectra of MgO'' and MgO\* samples / Spectrele FTIR ale probelor MgO'' și MgO\*.

**Table 2**  
XRF data of MgO''-Me, MgO\*-Me (Me = Ni, Cu) nanocomposites / Datele XRF ale nanocompozitelor MgO''-Me, MgO\*-Me (Me = Ni, Cu)

| Sample/Composition | % at  |
|--------------------|-------|
| <b>MgO''-Ni</b>    |       |
| MgO                | 81.72 |
| Ni                 | 18.28 |
| <b>MgO*-Ni</b>     |       |
| MgO                | 81.51 |
| Ni                 | 18.49 |
| <b>MgO''-Cu</b>    |       |
| MgO                | 80.44 |
| Cu                 | 19.56 |
| <b>MgO*-Cu</b>     |       |
| MgO                | 80.03 |
| Cu                 | 19.97 |

in Table 3.

It can be observed that the BET surface area values of MgO'' and MgO\* are 124 and 135 m<sup>2</sup>/g respectively. In the case of nanocomposites obtained based on MgO'' and MgO\* a decrease of specific surface area was observed. The specific surface area is well correlated with the crystallite size.

The shape of the loops of capillary-condensation hysteresis of isotherms in the field of adsorption indicates that the samples contain pores equivalent to both cylindrical and slit-like mesopores at the same time. The pore size distribution curve of the magnesium oxide powder that was obtained by the deposition method (Fig. 3 d, curve 1) shows mesopore homogeneity of the initial powder with a maximum of 30 nm; after adding nanoparticles, the pore size distribution becomes bimodal at maximum of 8.4 and 34 nm for the MgO''-Ni composite, 3.3 and 35 nm for the

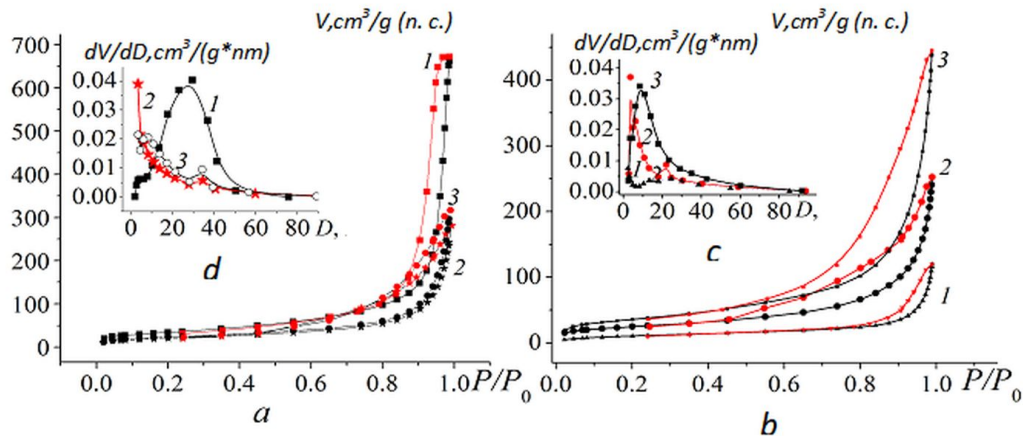


Fig. 3 - Isotherms of low-temperature adsorption-desorption of nitrogen (a, b) and differential pore size distributions in linear form (c, d) of nanocomposites based on MgO obtained by the precipitation method (a, d) and glycine-citrate nitrate method (b, c) 1 - without metals; 2 - with the addition of nickel; 3 - with the addition of copper / *Izotermele de adsorbție-desorbție ale azotului la temperatură joasă (a,b) și distribuțiilor diferențiale liniare ale dimensiunii porilor (c,d) ale nanocompozitelor pe bază de MgO obținut prin metoda de precipitare (a,d) și metoda glicina-citrat (b,c) 1-fără metale; 2-cu adaos de nichel; 3-cu adaos de cupru.*

**Table 3**  
Specific surface area ( $A_{BET}$ ), total pore volume ( $V_{sp des}$ ), and average pore diameter ( $D_{sp des}$ ) of MgO obtained by both methods and MgO\*-Me, MgO\*-Me (Me = Ni, Cu) nanocomposites / *Suprafața specifică ( $A_{BET}$ ), volumul total de pori ( $V_{sp des}$ ) și diametrul mediu al porilor ( $D_{sp des}$ ) ale MgO obținut prin ambele metode și nanocompozitelor MgO \*-Me, MgO \*-Me (Me = Ni, Cu)*

| Sample               | $A_{BET}$ , $m^2/g$ | $V_{sp des}$ , $cm^3/g$ | $D_{sp des}$ , nm |
|----------------------|---------------------|-------------------------|-------------------|
| MgO <sup>o</sup>     | 124                 | 1.038                   | 35                |
| MgO <sup>o</sup> -Cu | 86                  | 0.468                   | 22                |
| MgO <sup>o</sup> -Ni | 75                  | 0.409                   | 23                |
| MgO <sup>*</sup>     | 135                 | 0.670                   | 24                |
| MgO <sup>*</sup> -Cu | 41                  | 0.173                   | 19                |
| MgO <sup>*</sup> -Ni | 89                  | 0.368                   | 17                |

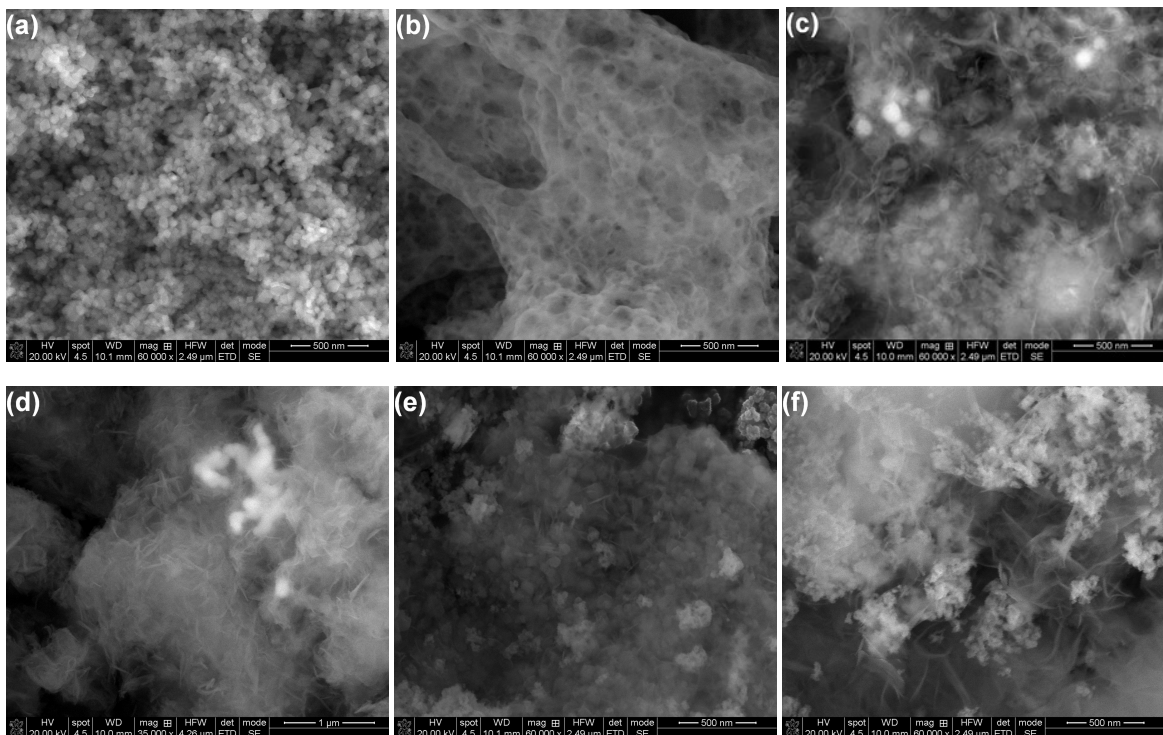


Fig. 4 - SEM images of MgO prepared by precipitation (a), combustion (b), impregnated with Ni (c, d) and Cu (e, f) nanoparticles / *Imaginile SEM ale MgO preparat prin precipitare (a), combustie (b), impregnat cu nanoparticule de Ni (c,d) și nanoparticule de Cu (e,f).*

MgO<sup>''</sup>-Cu composite. In the case of using the matrix of MgO carrier that was obtained by glycine-citrate-nitrate method (Fig. 3c), the initial powder was characterized by a disordered structure with a wide pore size distribution. With the introduction of nickel, four characteristic peaks appeared - at 3, 5, 6, and 22 nm, while MgO<sup>\*</sup>-Cu sample was characterized by a mono-modal distribution with a maximum of 8.4 nm. The specific surface values for MgO-based nanocomposites significantly decreased (1.4–1.7 times) upon the introduction of metals. The decrease of the specific surface area of the nanocomposites indicates that a certain fraction of metal nanoparticles size blocks the necks of cylindrical and slit-like pores, thereby reducing their availability for adsorbent molecules (nitrogen). Large particles of zero valence metals and their agglomerates act as intercalating agents for the lamellar structure of magnesium oxide. Thus, we can assume the formation of a hybrid, micro-mesoporous nanocomposite structure. This assumption is also confirmed by the appearance of bimodality on the BJH curves of samples.

### 3.5. SEM

The SEM images presented in Figure 4 show a different morphology of the MgO powder obtained by the two methods of preparation. In the case of samples prepared by precipitation method, nanometric particles (20-60nm) are obtained in a rather uniform granular domain and appear well crystallized (Fig 4a). In the case of MgO obtained by the combustion method, a porous morphology can be seen which is the result of the elimination of gases during the short reaction time (fig.4b). Mg(OH)<sub>2</sub> has the appearance of agglomerated particles in the SEM image Fig.4d and flake-like in SEM image Fig.4f. It is noteworthy to mention that the MgO<sup>\*</sup>-Ni sample presents a versatile morphology and in which Mg(OH)<sub>2</sub> is predominant [16]. Several reports demonstrated that these structures can be converted into each other (i.e. MgO - Mg(OH)<sub>2</sub>) by hydration procedures [18]. In general, the final properties of the nanocrystals strongly depend on their shape, agglomeration state and preparation process.

### 3.6 UV-Vis spectroscopy

UV-Vis spectra of modified samples with metals (Ni, Cu) (Fig.5) show a red shifted absorption band in comparison with MgO samples. For Ni modified catalysts it was observed a wide band at 390 nm associated to [Ni(H<sub>2</sub>O)<sub>6</sub>]<sup>2+</sup> ion. The band located at 660 nm is related to Ni<sup>2+</sup> species with distorted tetrahedral symmetry [Ni<sup>2+</sup>O<sub>4</sub>]<sup>2-</sup> and the one from 755 nm corresponds to Ni<sup>2+</sup> distorted octahedral symmetry [Ni<sup>2+</sup>O<sub>6</sub>]<sup>2-</sup> [18]. For Cu modified samples, UV-Vis spectra showed a wide signal obtained by overlapping of several absorption bands assigned to different states of supported copper. The absorption bands at 250 nm

correspond to Cu<sup>+</sup> species, the ones at 320–370 nm and 400–440 nm are related to charge transfer of O–Cu–O and Cu–O–Cu complexes, while the band at around 520–580 nm is specific for plasmon resonance effect of Cu<sub>n</sub> and the band at 620–850 nm is associated with Cu<sup>2+</sup> ions, the signal corresponding to d–d transitions [19].

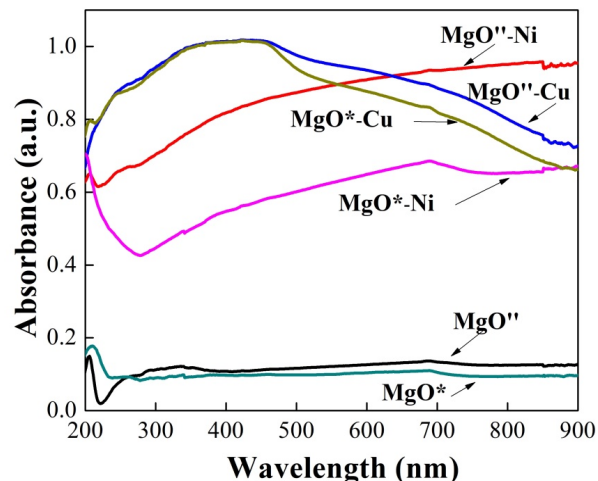


Fig. 5 - UV-Vis spectra of photocatalysts based on MgO  
Spectrele UV-Vis ale fotocatalizatorilor pe bază de MgO.

The band gap value was determined from the intersection of tangent through the point of inflexion in the absorption band and the photon energy axis. The values of the bad gap energy are show in Table 4. Metal ions narrow the band gap of MgO and improve the absorption. Comparing the band gap energy of MgO and MgO modified with Ni or Cu can be observed a shift toward visible light region. The high value of band gap in the case of MgO<sup>\*</sup>-Ni (5.6 eV) may be explain by the presence of Mg(OH)<sub>2</sub> and a possible oxidation of Ni to NiO. The experimental band gape of NiO is reported to be 4.3 eV [20]

Table 4

| Band gap energy of photocatalysts<br><i>Energia benzii interzise a fotocatalizatorilor</i> |         |
|--|---------|
| Sample   | Eg (eV) |
| MgO''  | 5.30    |
| MgO*   | 5.40    |
| MgO''-Ni   | 1.03    |
| MgO*-Ni  | 5.60    |
| MgO''-Cu   | 1.98    |
| MgO*-Cu  | 2.05    |

### 3.7. Photocatalytic activity evaluation

The photocatalytic performances of synthesized materials based on MgO modified with Ni and Cu were measured in degradation of AMX are shown in Fig. 6

The higher photodegradation efficiency towards AMX was observed for samples synthesized by precipitation method (MgO''-Ni and MgO''-Cu). The highest photodegradation efficiency of 65% was obtained for MgO''-Ni sample with the lowest band gap value, as it could be seen in

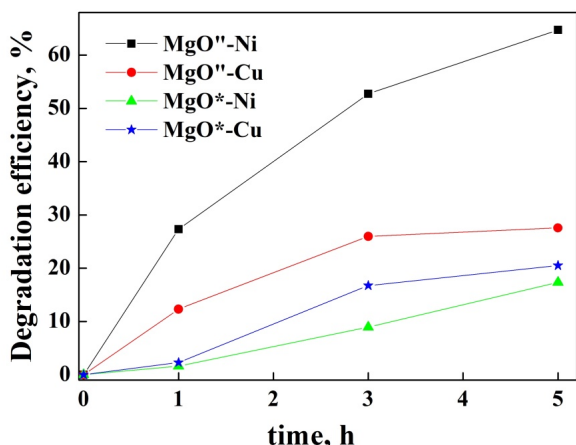


Fig 6 - Photocatalytic degradation of amoxicillin using synthesized materials / *Degradarea fotocatalitică a amoxicilinei folosind materiale sintetizate.*

Table 4. It is known that photocatalytic performances are related to physicochemical properties (e.g. surface area, pore size and volume, crystallite size) of the materials used in reaction, but for MgO catalyst no direct correlation was evidenced between them and the photocatalytic performances [21]. As it was previously reported by our group [20], AMX degradation takes place under strong oxidizing ability of OH<sup>·</sup> and O<sub>2</sub><sup>·-</sup> species generated on the support surface. These reactive oxygen species are generated through the reduction of O<sub>2</sub> adsorbed on MgO surface by the electrons from the conduction band (CB) of MgO [21]. It is well-known that degradation efficiency is a result of the presence of both radicals as well as the high adsorption ability of pollutant on the photocatalyst surface. It was evidenced that a high adsorption capacity leads to a higher degradation efficiency of amoxicillin (100%) [22]. Regarding MgO photocatalyst, the absorption of amoxicillin molecules is associated with the presence of basic sites on its surface, AMX being a weak acid molecule [23].

#### 4. Conclusion

In summary, nanocomposites based on MgO support, synthesized by two preparation methods (precipitation and combustion), and metal nanoparticles (Cu, Ni) were obtained.

The synergistic properties due to interfacial interaction between MgO support and metal nanoparticles influence the photocatalytic performance of the samples.

The morphology of the samples is strongly influenced by the preparation routes: the precipitation method supply well crystallized MgO nanoparticle in a narrow range of dimensions (30-60nm) while combustion method develops porous structures and lower crystallinity. However, MgO is chemically and texturally not stable upon storage in air and secondary phases can appear (e.g. Mg(OH)<sub>2</sub> and MgCO<sub>3</sub>). Deposition of the metallic

nanoparticles reduces specific surface and porosity of MgO.

MgO<sup>\*</sup>-Ni sample with the lowest band gap value of 1.03 eV exhibits the highest photodegradation efficiency towards AMX.

The results are promising, and the nanocomposites obtained and investigated in this paper may have potential applications in the wastewaters decontamination treatment.

#### Acknowledgment

The authors gratefully acknowledge the support from the Joint Research Project for Research Mobility between Romanian Academy and Belarus Academy of Science. I.V. Matsukevich, I. Atkinson contributed equally to this work

#### REFERENCES

- [1] X. Zhenga, K. Wanga, Z. Huanga, Y. Liua, J. Wenb, H. Peng, MgO nanosheets with N-doped carbon coating for the efficient visible-light photocatalysis, *Journal of Industrial and Engineering Chemistry*, 2029, **76**, 288.
- [2] L. Ge, W. Wang, Z. Peng, F. Tan, X. Wang, J. Chen, X. Qiao, Facile fabrication of Fe@MgO magnetic nanocomposites for efficient removal of heavy metal ion and dye from water, *Powder Technology*, 2028, **326**, 393.
- [3] S. Yousefi, B. Ghasemi, M. Tajally, A. Asghari, Optical properties of MgO and Mg(OH)<sub>2</sub> nanostructures synthesized by a chemical precipitation method using impure brine, *Journal of Alloys and Compounds*, 2017, **711**, 521.
- [4] A. Ansari, A. Ali, M. Asifa, Shamsuzzaman, Microwave-assisted MgO NP catalyzed one-pot multicomponent synthesis of polysubstituted steroidal pyridines, *New Journal of Chemistry*, 2018, **42**, 184.
- [5] V. Stengl, S. Bakardjeva, M. Marikova, P. Bezdi cka, J. Subrt, Magnesium oxide nanoparticles prepared by ultrasound enhanced hydrolysis of Mg-alkoxides, *Material Letters*, 2003, **57**, 3998.
- [6] R. Mbarki, A.H. Hamzaoui, A. Mnif, Dielectric properties and electrical conductivity of MgO synthesized by chemical precipitation and sol-gel method, *European Physics Journal Applied Physics*, 2015, **69**, 10402.
- [7] L. Todan, T. Dăscălescu, S. Preda, C. Andronescu, C. Munteanu, D.C. Culiță, A. Rusu, R. State, M. Zaharescu, Porous nanosized oxide powders in the MgO-TiO<sub>2</sub> binary system obtained by sol-gel method, *Ceramics International*, 2014, **40**, 15693.
- [8] M. Crișan, A. Jitianu, D. Crișan, M. Bălășoiu, N. Drăgan, M. Zaharescu, Sol-gel monocomponent nano-sized oxide powders, *Journal of Optoelectronic and Advanced Materials*, 2000, **2**, 339.
- [9] A. Sierra-Fernandez, L.S. Gomez-Villalba, O. Milosevic, R. Fort, M. E. Rabanal, Synthesis and morpho-structural characterization of nanostructured magnesium hydroxide obtained by a hydrothermal method, *Ceramics International*, 2014, **40**, 12285.
- [10] S. Chae, H. Lee, P.V. Pikhitsa, C. Kim, S. Shin, D. H. Kim, M. Choi, Synthesis of terraced and spherical MgO nanoparticles using flame metal combustion, *Powder Technology*, 2016, **305**, 132.
- [11] N. M. Julkapli, S. Bagheri, Magnesium oxide as a heterogeneous catalyst support. *Reviews in Inorganic Chemistry*, 2016, **36** (1), 1-41.
- [12] E. Norabadi, F. Kord Mostafapour, H. Kamani, E. Bazrafshan, S. D. Ashrafi, K. Pirasteh, M. Dashtizadeh, Photocatalytic process using magnesium oxide nanoparticles for amoxicillin removal from aqueous solution, *Journal of Torbat Heydariyeh University of Medical Sciences*, 2018, **6**(3), 1-12.
- [13] Y. Zheng, L. Cao, G. Xing, Z. Bai, J. Huang, Z. Zhang, Microscale flower-like magnesium oxide for highly efficient photocatalytic degradation of organic dyes in aqueous solution, *RSC Advances*, 2019, **9**, 7338.

- [14] N. F. Chayed, N. Kamarulzaman, N. Badar, K. Elong, Effect of Cu Doped in MgO on Nanostructures and their Band Gap Energies, *Solid State Phenomena*, 2019, **290**, 323.
- [15] M. Rezaei, M. Khajenoori, B. Nematollahi, Synthesis of high surface area nanocrystalline MgO by pluronic P123 triblock copolymer surfactant, *Powder Technology*, 2011, **205**, 112.
- [16] L. Kumari, W.Z. Li, C. H. Vannoy, R. M. Leblanc, D. Z. Wang, Synthesis, characterization and optical properties of Mg(OH)<sub>2</sub> micro-/nanostructure and its conversion to MgO, *Ceramics International*, 2009, **35**, 3355.
- [17] J. Green, Calcination of precipitated Mg(OH)<sub>2</sub> to active MgO in the production of refractory and chemical grade MgO, *Journal of Materials Science*, 1983, **18**, 637.
- [18] A. Guevara-Lara, A. E. Cruz-Perez, Z. Contreras-Valdez, J. Mogica-Betancourt, A. Alvarez-Hernandez, M. Vrinat, Effect of Ni promoter in the oxide precursors of MoS<sub>2</sub>/MgO–Al<sub>2</sub>O<sub>3</sub> catalysts tested in dibenzothiophene hydrodesulphurization, *Catalysis Today*, 2010, **149**, 288.
- [19] A. N. Pestryakov, V. P. Petranovskii, A. Kryazhov, O. Ozhereliev, N. Pfänder, A. Knop-Gericke, Study of copper nanoparticles formation on supports of different nature by UV–Vis diffuse reflectance spectroscopy, *Chemical Physics Letters*, 2004, **385** (3–4), 173.
- [20] G. A. Sawatzky, J. W. Allen, Magnitude and Origin of the Band Gap in NiO, *Physical Review Letters*, 1984, **53**, 2339.
- [21] Y. Zheng, L. Cao, G. Xing, Z. Bai, J. Huang, Z. Zhang, Microscale flower-like magnesium oxide for highly efficient photocatalytic degradation of organic dyes in aqueous solution, *RSC Adv.*, 2019, **9**, 7338.
- [22] G. Petcu, E. M. Anghel, S. Somacescu, S. Preda, D. C. Culita, S. Mocanu, M. Ciobanu, V. Parvulescu, Hierarchical Zeolite Y Containing Ti and Fe Oxides as Photocatalysts for Degradation of Amoxicillin, *J. Nanosci. Nanotechnol.*, 2020, **20**, 1158.
- [23] J. S. Kwak, K. R. Oh, K. Y. Kim, J. M. Lee, Y. U. Kwon, CO<sub>2</sub> absorption and desorption characteristics of MgO-based absorbent promoted by triple eutectic alkali carbonate, *Physical Chemistry Chemical Physics*, 2019, **21**(37), 20805.

\*\*\*\*\*

## 101 de ani de la MAREA UNIRE : 1918 - 2019



*Catedrala Ortodoxă a "Reîntregirii Neamului", locul unde au fost încoronăți Ferdinand, primul Rege al României Mari și Regina Maria, la 15 octombrie 1922.*

La 1 decembrie 1918, la Alba Iulia peste 100.000 de oameni veniți din toate localitățile au aclamat Unirea. În "Sala Unirii" delegații Marii Adunări Naționale, în număr de 1228 au hotărât Unirea Transilvaniei, Banatului, Crișanei și Maramureșului cu țara mamă, România.

\*\*\*\*\*